

Finite transverse conductance and anisotropic magnetoconductance under an applied in-plane magnetic field in two-dimensional electron gases with strong spin-orbit coupling

Abhiram Soori^{1,*}

¹*School of Physics, University of Hyderabad, C. R. Rao Road, Gachibowli, Hyderabad-500046, India*

The current in response to a bias in certain two-dimensional electron gas (2DEG), can have a nonzero transverse component under a finite magnetic field applied in the plane where electrons are confined. This phenomenon known as planar Hall effect is accompanied by dependencies of both the longitudinal and the transverse components of the current on the angle ϕ between the bias direction and the magnetic field. This effect can be observed in a variety of systems, for example in topological insulators where spin-momentum locking of the topologically protected surface states is the root cause for the effect and in magnetic systems where anisotropic magnetic ordering induces it. In 2DEG with spin orbit coupling (SOC) such as oxide interfaces, this effect has been experimentally witnessed. Further, a fourfold oscillation in longitudinal resistance as a function of ϕ has also been observed. Motivated by these, we perform scattering theory calculations on a 2DEG with SOC in presence of an in-plane magnetic field connected to two dimensional leads on either sides to obtain longitudinal and transverse conductances. We find that the longitudinal conductance is π -periodic and the transverse conductance is 2π -periodic in ϕ . The magnitude of oscillation in transverse conductance with ϕ is enhanced in certain patches in (α, b) -plane where α is the strength of SOC and b is Zeeman energy due to magnetic field. The oscillation in transverse conductance with ϕ can be highly multi-fold for large values of α and b . The highly multi-fold oscillations of transverse conductance are due to Fabry-Pérot type interference between the modes in the central region as backed by its length dependent features. Our study establishes that SOC in a material is sufficient to observe planar Hall effect without the need for anisotropic magnetic ordering or nontrivial topology of the bandstructure.

I. INTRODUCTION

The longitudinal and the Hall resistances in Hall measurements of certain systems in presence of a magnetic field applied in the same plane as Hall measurements depend on the angle between magnetic field and the longitudinal direction. Such a dependence of the longitudinal resistance/conductance is called anisotropic magneto-resistance/conductance, whereas such a dependence of the Hall resistance is called planar Hall effect. The anisotropic magnetoresistance (AMR) and planar Hall effect (PHE) have been observed in a variety of magnetic systems¹⁻⁴. Recently PHE has also been observed in magnetic skyrmion systems⁵. PHE amplitude in certain magnetic systems is sensitive to magnetic fields as low as earth's magnetic field³. Recently, experimental investigations of AMR and PHE have been in exotic topological materials such as topological insulators⁶⁻⁹ and Weyl semimetals^{10,11}. A common physical factor among topological materials is spin momentum locking which has origins in strong spin orbit coupling (SOC) of the constituent atoms^{12,13}. The SOC in the bulk of topological insulators such as Bi₂Se₃ is Dresselhaus like which results in topologically protected surface states that possess spin-momentum locking¹². The spin-momentum locking is responsible for PHE and AMR in topological insulators¹⁴. A natural question that arises is: 'does a system with SOC alone, but topologically trivial exhibit PHE and AMR?' It is therefore interesting to investigate AMR and PHE in two-dimensional electron systems with SOC.

A two dimensional electron gas (2DEG) with SOC is

an ideal platform for the realization of Datta-Das transistor proposed in 1990¹⁵. But such systems are not easy to achieve experimentally since existence of Rashba spin split bands alone with large enough SOC strength is rare. In 2015, Datta-Das transistor was realized experimentally in InGaAs/InAlAs heterostructures¹⁶. Recently, Bi₂Se₃/MoTe₂ heterostructure has been proposed to be a 2DEG with large SOC strength¹⁷. Another 2DEG with large SOC strength is LaAlO₃/SrTiO₃ interface where the strength of SOC can be further controlled by an applied gate voltage⁴. In addition to SOC, there are localized magnetic impurities that determine the transport behavior in this system. This system exhibits PHE and a peculiar type of AMR. The AMR oscillation is fourfold when the electrons confined at the interface is purely two-dimensional whereas it is twofold when the interfacial electrons have access to three dimensions. Also, AMR has been extensively studied in LaAlO₃/SrTiO₃ interface¹⁸ and in SrTiO₃¹⁹. PHE and AMR have been observed recently at the interface of LaVO₃-KTaO₃ which hosts electrons confined to two dimensions with large SOC²⁰. In this system, the AMR oscillation is twofold at low magnetic fields whereas it is fourfold at high magnetic fields. AMR has been investigated in 2DEG with SOC in a number of studies²¹⁻²⁴, taking into account scattering from impurities. But a theoretical study of PHE in 2DEG with SOC is missing.

In this work, we study transport across a 2DEG with SOC in presence of a magnetic field applied in the same plane as 2DEG, connected to two-dimensional leads on either sides as shown in fig. 1. We follow the scatter-

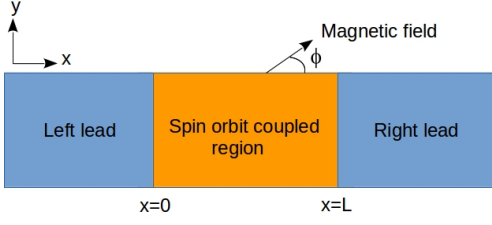


FIG. 1. Schematic diagram of the setup under study. The region in the middle from $x = 0$ to $x = L$ is the region with spin-orbit coupling and an in-plane magnetic field which makes an angle ϕ with the longitudinal direction. A bias is applied from left lead to right lead.

ing theory approach developed in a recent work in the context of topological insulators¹⁴ to study AMR and PHE quantitatively by calculating the longitudinal and transverse conductances. The difference between this approach and the experiments is that here the components of the current in the longitudinal and transverse directions in response to the bias in longitudinal direction are determined whereas in experiments, voltages developed in longitudinal and transverse directions in response to current in longitudinal direction are measured. In this paper, we present the details of calculation in section II and present the results accompanied by an analysis in section III. In section IV, we discuss the main results and conclude.

II. DETAILS OF CALCULATION

The Hamiltonian for the system under study is

$$H = \left[-\frac{\hbar^2}{2m} \left(\frac{\partial^2}{\partial x^2} + \frac{\partial^2}{\partial y^2} \right) - \mu \right] \sigma_0 + \Delta_L(x) \left[i\alpha \left(\sigma_y \frac{\partial}{\partial x} - \sigma_x \frac{\partial}{\partial y} \right) + b(\cos \phi \sigma_x + \sin \phi \sigma_y) \right], \quad (1)$$

where $\Delta(x) = \Theta(x)\Theta(L-x)$ and Θ is Heavyside step function. Here, m is the effective mass of electrons in the system, μ -the chemical potential, α -the strength of SOC, b -the magnitude of the Zeeman energy due to the magnetic field, ϕ -the angle made by the in-plane magnetic field with the x -axis and σ_x, σ_y are Pauli spin matrices. The SOC and the magnetic field are present only in the region $0 < x < L$, and the regions to the left and right model the leads. The length of the system in y -direction is L_y and the limit $L_y \rightarrow \infty$ is taken along with periodic boundary condition in y -direction. We do not assume any barrier at the interfaces $x = 0, L$. The boundary conditions at $x = 0, L$ are different from the conventional continuities of the wavefunction ψ and its derivative $\partial_x \psi$. These boundary conditions can be derived by demanding the conservation of the x -component of current at the junctions $x_0 = 0, L$. One choice of the

boundary conditions is the continuity of the wavefunction ψ accompanied by

$$\partial_x \psi|_{x_0^-} = \partial_x \psi|_{x_0^0} - \frac{i\alpha m}{\hbar^2} \sigma_y \psi|_{x_0^0}, \quad (2)$$

where $s_0 = \text{sign}(L/2 - x_0)$ and $x_0^0 = \lim_{\epsilon \rightarrow 0^+} [x_0 + s_0 \epsilon]$. The dispersion in the regions $x < 0$ and $x > L$ are $E = \hbar^2(k_x^2 + k_y^2)/2m - \mu$, while the dispersion in the central region ($0 < x < L$) is: $E = \hbar^2(k_x^2 + k_y^2)/2m - \mu \pm \sqrt{(b \cos \phi + \alpha k_y)^2 + (b \sin \phi - \alpha k_x)^2}$. The wavefunction at energy E of an incident σ -spin electron from the left lead at an angle θ with x -axis has the form $e^{ik_y y} \psi_\sigma(x)$, where

$$\begin{aligned} \psi_\sigma(x) &= e^{ik_x x} |\sigma\rangle + \sum_{\sigma'=\uparrow, \downarrow} r_{E, \sigma' \sigma} e^{-ik_x x} |\sigma'\rangle, \quad \text{for } x < 0, \\ &= \sum_{j=1}^4 s_{E, j, \sigma} e^{ik'_{xj} x} [u_j, v_j]^T, \quad \text{for } 0 < x < L, \\ &= \sum_{\sigma'=\uparrow, \downarrow} t_{E, \sigma' \sigma} e^{ik_x x} |\sigma'\rangle, \quad \text{for } x > L, \end{aligned} \quad (3)$$

$k_y = \sqrt{2m\mu} \sin \theta / \hbar$, $k_x = \sqrt{2m\mu} \cos \theta / \hbar$, σ' is the spin opposite to σ , $|\uparrow\rangle = [1, 0]^T$, $|\downarrow\rangle = [0, 1]^T$ and k'_{xj} (for $j = 1, 2, 3, 4$) are four roots of the dispersion of the central region for k_x at the given E and k_y . Due to translational invariance in y -direction, k_y is same in all the regions. The current component along x -direction is same everywhere whereas the current component along y -direction can vary as a function of spatial location x . In the region $0 < x < L$, at location x , the y -component of current due to an incident σ -spin electron at energy E that makes an angle θ with x -axis is:

$$I_{y, \sigma}(E, \theta, x) = e \left[\frac{\hbar k_y}{m} \psi_\sigma^\dagger(x) \psi_\sigma(x) + \frac{\alpha}{\hbar} \psi_\sigma^\dagger(x) \sigma_x \psi_\sigma(x) \right], \quad (4)$$

where e is the electron charge. Let $[I_x, I_y(x)]$ be the current flowing at x in response to a voltage bias in applied in the window $(0, eV)$. Then, the differential- longitudinal and transverse conductances are $G_{xx} = dI_x/dV$ and $G_{yx}(x) = dI_y(x)/dV$ which can be expressed as

$$\begin{aligned} G_{xx} &= \frac{\sqrt{2m(\mu_N + eV)}}{\hbar} \frac{e^2}{h} L_y \sum_{\sigma, \sigma'} \int_{-\pi/2}^{\pi/2} d\theta \cos \theta |t_{\sigma', \sigma}|^2, \\ G_{yx}(x) &= \frac{e}{h} \frac{m L_y}{\hbar} \sum_{\sigma} \int_{-\pi/2}^{\pi/2} d\theta I_{y, \sigma}(eV, \theta, x), \quad \text{for } 0 < x < L, \\ G_{yx}(x) &= \frac{e^2}{h} L_y \sum_{\sigma, \sigma'} \int_{-\pi/2}^{\pi/2} d\theta k_y |t_{\sigma', \sigma}|^2, \quad \text{for } x > L. \end{aligned} \quad (5)$$

The dependence of G_{xx} on ϕ is termed anisotropic magnetoconductance (AMC) and the dependence of G_{yx} on ϕ is termed PHE. PHE amplitude is defined as half the difference between maximum and minimum values of G_{yx} when ϕ is varied.

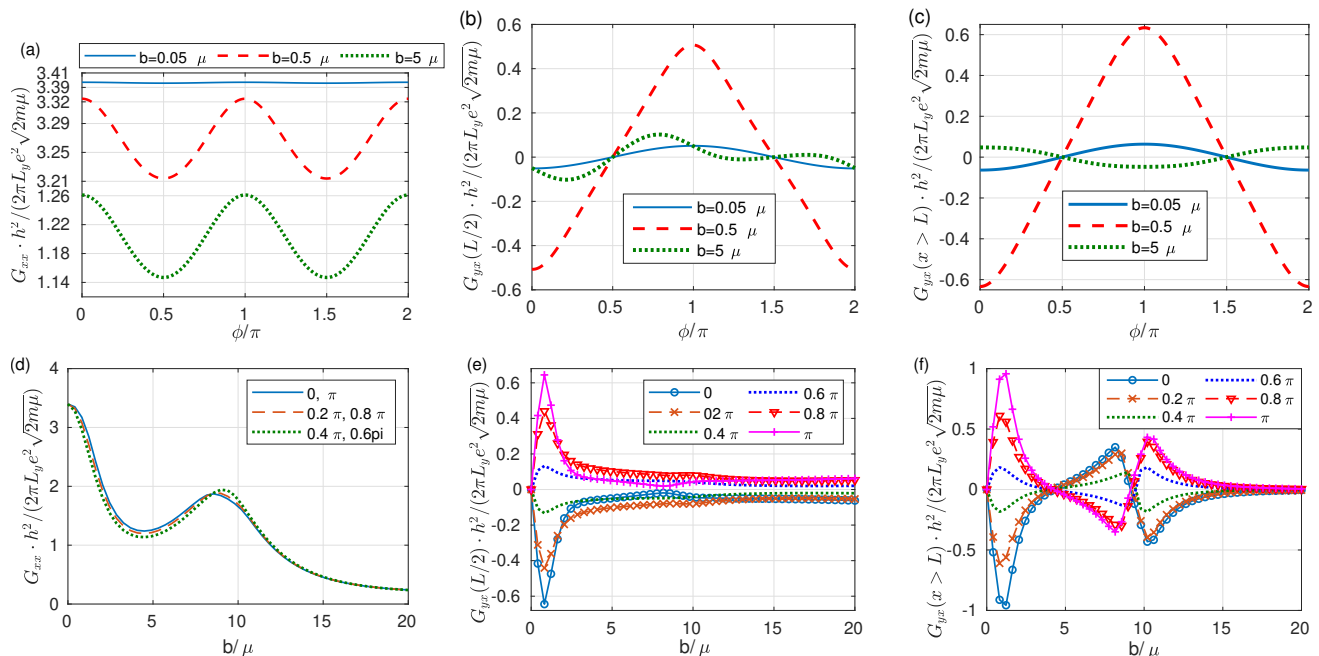


FIG. 2. Anisotropic magnetoconductance and planar Hall effect. (a) The longitudinal conductance, and the transverse conductances: at (b) $x = L/2$ and in the region (c) $x > L$ as plotted as functions of ϕ - the angle between applied in-plane magnetic field and the longitudinal direction. In (a), different curves are displaced along y so as to fit all curves in the same graph and show the dependence of G_{xx} with ϕ . In doing so, the values on y -axis are also relabeled - the gaps in ranges of y axis (1.26, 3.21) and (3.32, 3.39) are not shown. In (d) longitudinal conductance, in (e) transverse conductance at $x = L/2$ and in (f) transverse conductance at $x > L$ are plotted as functions of b for different choices of angles ϕ mentioned in the plot legend. Parameters: $\alpha = \hbar\sqrt{\mu/(2m)}$, $L = \hbar/\sqrt{2m\mu}$.

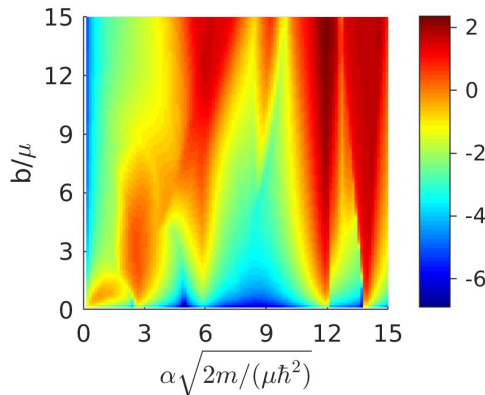


FIG. 3. Logarithm of PHE amplitude evaluated at $x = L/2$ as a function of b and α . $L = \hbar/\sqrt{2m\mu}$.

III. RESULTS AND ANALYSIS

Parameters in the Hamiltonian eq. (1) are m , μ , L , α and b . All parameters apart from m and μ are expressed in terms of these two parameters. L is taken to be $\hbar\sqrt{2m\mu}$, except when mentioned specifically. Since

current along x -axis is conserved, the longitudinal conductance G_{xx} is same at all locations x . But the transverse conductance G_{yx} is a function of the spatial location x . All the conductances calculated in this work are at zero bias (i.e., at $E = 0$). In Fig. 2(a,b,c), we plot G_{xx} , $G_{yx}(L/2)$ and $G_{yx}(x > L)$, all at zero bias as functions of ϕ respectively at different strengths of the magnetic field labeled in the legend. From fig. 2(a), we can see that for low magnetic fields, the amplitude of variation in AMC is small and it increases with magnetic field accompanied by a decrease in the mean value of AMC. The mean value of AMC decreases with magnetic field since a higher magnetic field implies a higher mismatch between the wavenumbers in different regions. In fig. 2(b,c) the transverse conductance shows oscillations of a higher magnitude for an intermediate magnetic field. At low magnetic fields, the transverse drift of the incident current is small whereas at large magnitudes of the magnetic field b , the SOC becomes relatively small leading to a lesser importance of spin being locked to the momentum. For $b = 5\mu$, we see that the transverse conductance at $x = L/2$ exhibits two-fold oscillation, whereas it is still one-fold at $x > L$. The sign of $G_{yx}(x > L)$ at $\phi = 0$ changes with magnetic field strength. For angles $\phi = \pi/2, 3\pi/2$, it can be seen from the system Hamiltonian that the system becomes symmetric under $y \rightarrow -y$. Hence, the transverse

conductance at these angles is exactly zero as can be seen in fig. 2(b,c). In fig. 2(d,e,f), we plot three conductances G_{xx} , $G_{yx}(x = L/2)$ and $G_{yx}(x > L)$ respectively as functions of b . The overall decrease in G_{xx} with increasing magnetic field is due to the increasing mismatch between the wavenumbers in different regions. But the local peak around $b \sim 9\mu$ is due to the Fabry-Pérot interference in the central region, which we have verified by changing the length L in the system. We see that the magnitude of transverse conductance at angles ϕ apart from $\pi/2, 3\pi/2$ first increases with magnetic field, reaches a peak and then decreases. We see that particularly the $G_{yx}(x > L)$ oscillates with b changing sign at certain values of b with an overall decrease in local peak. Such oscillations in $G_{yx}(x > L)$ with b are due to Fabry-Pérot type interference in the central region as can be verified by varying the length L ^{25–28}.

In Fig. 3, we show a color plot of the logarithm of PHE amplitude evaluated at $x = L/2$ as a function b and α , keeping the other parameters the same. We see multiple patches in (α, b) -plane where PHE amplitude is high. The transverse conductance at $x > L$ shows interesting features in these regions. In the patch between $0 < \alpha\sqrt{2m}/(\mu\hbar^2) \lesssim 2$, $G_{yx}(x > L)$ shows one-fold oscillation similar to the one in fig. 2(c), whereas G_{xx} shows two-fold oscillations. In the high PHE amplitude patch in the range $2 \lesssim \alpha\sqrt{2m}/(\mu\hbar^2) \lesssim 4$, the oscillation of $G_{yx}(x > L)$ with ϕ is one-fold at low b ($b \leq \mu$) and becomes three-fold in the middle of the patch as b lies in the range $(2, 6)\mu$. At higher values of b in this range of α , $G_{yx}(x > L)$ is one-fold. Here, we use the term n -fold for the oscillation of $G_{yx}(x > L)$ with ϕ if the value of $G_{yx}(x > L)$ crosses the mean value of $G_{yx}(x > L)$ (which is 0) $2n$ -times as ϕ is varied across the range $[0, 2\pi]$. We now explore the narrow patch around $\alpha\sqrt{2m}/(\mu\hbar^2) \sim 9$ in fig. 4. We can see that as b/μ increases from 6 to 16, the oscillation in $G_{yx}(x > L)$ changes from being one-fold to seven-fold. For the choice of $b/\mu = 6, 10, 14, 16$ the oscillation in $G_{yx}(x > L)$ is one-, three-, five-, seven-fold respectively. For the same set of parameters, the longitudinal conductance G_{xx} shows a number of local peaks as a function of ϕ that increases with b as can be seen in fig. 5. For choices of $b/\mu = 6, 10, 14, 16$, G_{xx} shows two, two, four, six local peaks respectively. This is a reflection of highly multi-fold oscillation in $G_{yx}(x > L)$ though not an exact one-to-one correspondence.

It is instructive to look at the evolution of the Fermi surface of the central region as the angle ϕ between longitudinal direction and the magnetic field is varied. For the choice of parameters $\alpha = 9\hbar\sqrt{\mu}/(2m)$ and $b = 14\mu$, we plot the Fermi surface for different choices of ϕ in the range $[0, 0.5\pi]$ in fig. 6, focusing on the range of k_y allowed by the leads. Outside this range of k_y , there is no scattering. Because of spin degree of freedom, there are two bands and hence we expect two Fermi surfaces. For small values of ϕ , there is only one Fermi surface in the focused range of k_y and the second (inner) Fermi surface appears in this range of k_y around $\phi \lesssim 0.3\pi$. For the

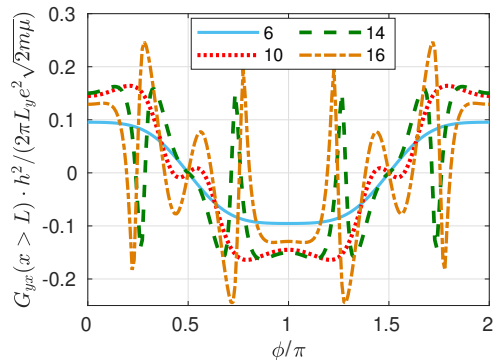


FIG. 4. $G_{yx}(x > L)$ plotted as a function of ϕ for the choice $\alpha = 9\hbar\sqrt{\mu}/(2m)$ and for different values of b/μ mentioned in the legend. $L = \hbar/\sqrt{2m\mu}$.

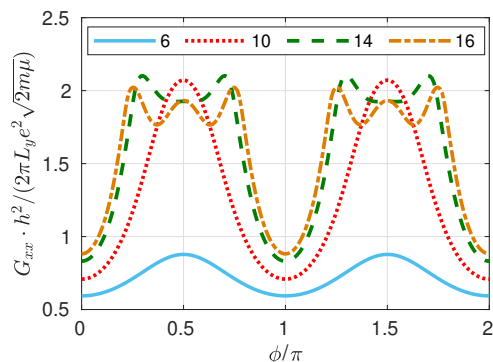


FIG. 5. G_{xx} plotted as a function of ϕ for different choices of b/μ shown in the legend for the same choice of parameters as in fig. 4.

choice $\phi = 0.5\pi$, the Fermi surfaces are symmetric about the line $k_y = 0$ and hence the transverse conductance is zero for this choice of ϕ . For other choices of ϕ , there exists asymmetry between modes at k_y and $-k_y$ as can be seen from this figure, and this is the root cause for finite transverse conductance.

Now we turn to the origin of high-fold oscillations in $G_{yx}(x > L)$ at large strengths of SOC and high magnetic fields. For a given ϕ and a given angle θ of incident electron, k_y is fixed and the transport problem at the heart of the phenomenon is that of transmission across a region of SOC and magnetic field in effectively one dimension. Hence, the transmission probability is determined by the interference condition which is more complex than the simpler condition for transmission across a one dimensional barrier $k_x''L = n\pi$, where k_x'' is the wavenumber in the barrier region. Further, the value of transverse conductance in the region $x > L$ is determined by adding k_y times the transmission probabilities over different angles of incidence θ . So, effectively we can write a Fabry-Pérot interference condition $k_x''(\phi, L)L = n\pi$, where $k_x''(\phi, L)$ depends on ϕ and L . For larger values of b and α , the

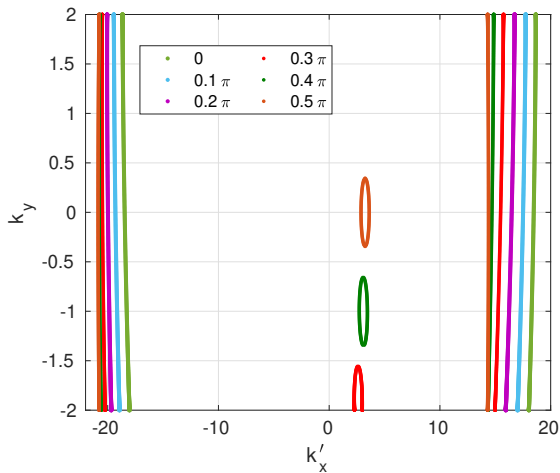


FIG. 6. Part of the Fermi surface plotted across a range of k_y that are allowed in the leads. Different curves are for different choices of ϕ as shown in the legend. $\alpha = 9\hbar\sqrt{\mu/(2m)}$ and $b = 9\mu$.

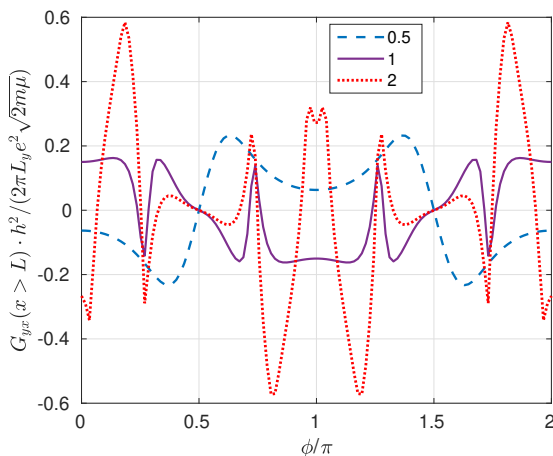


FIG. 7. $G_{yx}(x > L)$ versus ϕ for different lengths L of the SOC region in the middle for $\alpha = 9\hbar\sqrt{\mu/(2m)}$ and $b = 9\mu$. Different curves are for different lengths of the central region indicated by the values of $L\sqrt{2m\mu}/\hbar$ in the plot legend.

variation of k_x'' with ϕ is more drastic and hence a higher-fold oscillation in $G_{yx}(x > L)$. The dependence of k_x'' on L is slow beyond a certain length since the transverse conductance is obtained by integrating over all angles of incidence. As L increases, $G_{yx}(x > L)$ is expected to show higher-fold oscillations as a function of ϕ . In fig. 7, we see higher-fold oscillation in $G_{yx}(x > L)$ as

L is increased in qualitative agreement with the above argument.

IV. DISCUSSION AND CONCLUSION

We have studied the phenomena of PHE and AMC in 2DEG with SOC. In magnetic materials, PHE occurs as a result of anisotropic magnetic texture^{1-3,5}. PHE observed in Weyl semimetals^{10,11,29} is attributed to the chiral anomaly which has origin in topology of the band-structure. In topological insulators, PHE is ascribed to contain the information about the topological surface state transport⁶. In topological insulators, PHE and AMR result from perfect spin-momentum locking in the topologically protected surface states¹⁴. In contrast, we have shown in this work that PHE and AMR can be observed in systems with SOC alone without the need for topological protection or magnetism. Further, we have shown that PHE can have a large magnitude at large values of SOC strength and magnetic field. At a given strength of SOC, at very small and very large magnetic fields, the PHE amplitude is small. When the PHE amplitude evaluated at $x = L/2$ is large, the oscillations in transverse conductance evaluated in the region $x > L$ can be highly multi-fold. We find one-, three-, five-, and seven-fold oscillations of the transverse conductance. This is in contrast to the fourfold oscillation of the AMR in systems with SOC^{4,20}. In the first place, PHE is due to breaking of the $y \rightarrow -y$ symmetry in the Hamiltonian when an in-plane magnetic field is applied in the region with SOC. Further, the highly multi-fold oscillations in transverse conductance is due to the Fabry-Pérot type interference in the central region. Such oscillations also show up in AMC, but to a lower degree. Our results do not apply to LaAlO₃/SrTiO₃ interface despite strong SOC since magnetic impurities are present in this system. PHE can be employed in detection of magnetic fields making the highly multi-fold oscillations useful in development of magnetic field sensors. PHE has not been widely observed in two-dimensional electron systems with SOC due to small strength of SOC. LaVO₃-KTaO₃ interface has been a promising two-dimensional system with SOC where PHE and AMR can be observed. We envisage many more two dimensional electron systems with large SOC in the years to come where PHE can be observed.

ACKNOWLEDGMENTS

The author thanks Dhavala Suri for useful discussions and DST-INSPIRE Faculty Award (Faculty Reg. No. : IFA17-PH190) for financial support.

* abhiraams@uohyd.ac.in

¹ A. M. Nazmul, H. T. Lin, S. N. Tran, S. Ohya, and M. Tanaka, "Planar hall effect and uniaxial in-plane mag-

- netic anisotropy in Mn δ -doped GaAs/*p*-AlGaAs heterostructures,” *Phys. Rev. B* **77**, 155203 (2008).
- ² J. Li, S. L. Li, Z. W. Wu, S. Li, H. F. Chu, J. Wang, Y. Zhang, H. Y. Tian, and D. N. Zheng, “A phenomenological approach to the anisotropic magnetoresistance and planar hall effect in tetragonal $\text{La}_{2/3}\text{Ca}_{1/3}\text{MnO}_3$ thin films,” *J. Phys.: Condens. Matter* **22**, 146006 (2010).
 - ³ A. Roy and P. S. A. Kumar, “Giant planar hall effect in pulsed laser deposited permalloy films,” *Journal of Physics D: Applied Physics* **43**, 365001 (2010).
 - ⁴ A. Annadi, Z. Huang, K. Gopinadhan, X. Renshaw Wang, A. Srivastava, Z. Q. Liu, H. Harsan Ma, T. P. Sarkar, T. Venkatesan, and Ariando, “Fourfold oscillation in anisotropic magnetoresistance and planar hall effect at the $\text{LaAlO}_3/\text{SrTiO}_3$ heterointerfaces: Effect of carrier confinement and electric field on magnetic interactions,” *Phys. Rev. B* **87**, 201102 (2013).
 - ⁵ M. Hirschberger, T. Nakajima, M. Kriener, T. Kurumaji, L. Spitz, S. Gao, A. Kikkawa, Y. Yamasaki, H. Sagayama, H. Nakao, S. Ohira-Kawamura, Y. Taguchi, T.-h. Arima, and Y. Tokura, “High-field depinned phase and planar hall effect in the skyrmion host Gd_2PdSi_3 ,” *Phys. Rev. B* **101**, 220401 (2020).
 - ⁶ A. A. Taskin, H. F. Legg, F. Yang, S. Sasaki, Y. Kanai, K. Matsumoto, A. Rosch, and Y. Ando, “Planar hall effect from the surface of topological insulators,” *Nat. Commun.* **8**, 1340 (2017).
 - ⁷ D. Rakhmilevich, F. Wang, W. Zhao, M. H. W. Chan, J. S. Moodera, C. Liu, and C.-Z. Chang, “Unconventional planar hall effect in exchange-coupled topological insulator–ferromagnetic insulator heterostructures,” *Phys. Rev. B* **98**, 094404 (2018).
 - ⁸ P. He, S. S.-L. Zhang, D. Zhu, S. Shi, O. G. Heinonen, G. Vignale, and H. Yang, “Nonlinear planar hall effect,” *Phys. Rev. Lett.* **123**, 016801 (2019).
 - ⁹ A. Bhardwaj, P. S. Prasad, K. Raman, and D. Suri, “Observation of planar hall effect in topological insulator – Bi_2Te_3 ,” arXiv: 2104.05246 (2021).
 - ¹⁰ A. A. Burkov, “Giant planar hall effect in topological metals,” *Phys. Rev. B* **96**, 041110 (2017).
 - ¹¹ N. Kumar, S. N. Guin, C. Felser, and C. Shekhar, “Planar hall effect in the weyl semimetal GdPtBi ,” *Phys. Rev. B* **98**, 041103 (2018).
 - ¹² X.-L. Qi and S.-C. Zhang, “Topological insulators and superconductors,” *Rev. Mod. Phys.* **83**, 1057–1110 (2011).
 - ¹³ N. P. Armitage, E. J. Mele, and A. Vishwanath, “Weyl and dirac semimetals in three-dimensional solids,” *Rev. Mod. Phys.* **90**, 015001 (2018).
 - ¹⁴ D. Suri and A. Soori, “Finite transverse conductance in topological insulators under an applied in-plane magnetic field,” arXiv: 2101.07670 (2021).
 - ¹⁵ S. Datta and B. Das, “Electronic analog of the electro-optic modulator,” *Appl. Phys. Lett.* **56**, 665 (1990).
 - ¹⁶ P. Chuang, S.-C. Ho, L. W. Smith, F. Sfigakis, M. Pepper, C.-H. Chen, J.-C. Fan, J. P. Griffiths, I. Farrer, H. E. Beere, G. A. C. Jones, D. A. Ritchie, and T.-M. Chen, “All-electric all-semiconductor spin field-effect transistors,” *Nature Nanotechnology* **10**, 35–39 (2015).
 - ¹⁷ T.-H. Wang and H.-T. Jeng, “Wide-range ideal 2d rashba electron gas with large spin splitting in $\text{Bi}_2\text{Se}_3/\text{MoTe}_2$ heterostructure,” *npj Computational Materials* **3**, 5 (2017).
 - ¹⁸ P. K. Rout, I. Agireen, E. Maniv, M. Goldstein, and Y. Dagan, “Six-fold crystalline anisotropic magnetoresistance in the (111) $\text{LaAlO}_3/\text{SrTiO}_3$ oxide interface,” *Phys. Rev. B* **95**, 241107 (2017).
 - ¹⁹ L. Miao, R. Du, Y. Yin, and Q. Li, “Anisotropic magnetotransport properties of electron gases at SrTiO_3 (111) and (110) surfaces,” *Applied Physics Letters* **109**, 261604 (2016).
 - ²⁰ N. Wadehra, R. Tomar, R. M. Varma, R. K. Gopal, Y. Singh, S. Dattagupta, and S. Chakraverty, “Planar hall effect and anisotropic magnetoresistance in polar-polar interface of $\text{LaVO}_3 - \text{KTaO}_3$ with strong spin-orbit coupling,” *Nat. Commun.* **11**, 874 (2020).
 - ²¹ C. M. Wang and M. Q. Pang, “Nonvanishing anisotropic magnetoresistance in rashba two-dimensional electron systems with nonmagnetic disorders,” *EPL* **88**, 27005 (2009).
 - ²² C. M. Wang, “Anisotropic magnetoresistance in a two-dimensional electron system with rashba and dresselhaus spin-orbit coupling,” *Phys. Rev. B* **82**, 165331 (2010).
 - ²³ C. M. Wang, “Anisotropic magnetoresistance in a rashba two-dimensional electron system: The role of nonmagnetic long-range scattering and nonparabolic energy band,” *EPL* **93**, 17005 (2011).
 - ²⁴ N. Boudjada, I. Khaït, and A. Paramekanti, “Anisotropic magnetoresistance in multiband systems: Two-dimensional electron gases and polar metals at oxide interfaces,” *Phys. Rev. B* **99**, 195453 (2019).
 - ²⁵ A. Soori, S. Das, and S. Rao, “Magnetic-field-induced fabry-pérot resonances in helical edge states,” *Phys. Rev. B* **86**, 125312 (2012).
 - ²⁶ A. Soori and S. Mukerjee, “Enhancement of crossed andreev reflection in a superconducting ladder connected to normal metal leads,” *Phys. Rev. B* **95**, 104517 (2017).
 - ²⁷ R. Nehra, D. S. Bhakuni, A. Sharma, and A. Soori, “Enhancement of crossed andreev reflection in a kitaev ladder connected to normal metal leads,” *J. Phys.: Condens. Matter* **31**, 345304 (2019).
 - ²⁸ A. Soori, “Transconductance as a probe of nonlocality of majorana fermions,” *J. Phys.: Condens. Matter* **31**, 505301 (2019).
 - ²⁹ S. Nandy, Girish Sharma, A. Taraphder, and S. Tewari, “Chiral anomaly as the origin of the planar hall effect in weyl semimetals,” *Phys. Rev. Lett.* **119**, 176804 (2017).